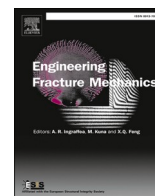




ELSEVIER

Contents lists available at ScienceDirect

Engineering Fracture Mechanics

journal homepage: www.elsevier.com/locate/engfracmech

Effect of the manufacturing parameters on the tensile and fracture properties of FDM 3D-printed PLA specimens

Liviu Marșavina^a, Cristina Vălean^{a,b,*}, Mihai Mărghițaș^a, Emanoil Linul^{a,*}, Seyed Mohammad Javad Razavi^c, Filippo Berto^c, Roberto Brighenti^d

^a Department of Mechanics and Strength of Materials, Politehnica University Timisoara, 1 Mihai Viteazu Blvd., Timisoara 300 222, Romania

^b Research Institute for Renewable Energies, Politehnica University Timisoara, Musicescu Gavril Str., No. 138, Timisoara 300 774, Romania

^c Norwegian University of Science and Technology (NTNU), Richard Birkelands vei 2b, 7491, Trondheim, Norway

^d University of Parma, Viale delle Scienze 181/A, 43124 Parma, Italy

ARTICLE INFO

Keywords:

FDM technique, process parameters
Tensile properties
mode I and II fracture toughness
Crack paths

ABSTRACT

Fused Deposition Modeling (FDM), also known as material extrusion, is currently one of the most popular Additive Manufacturing (AM) technology on the market. In this study, two commercial FDM printers (Prusa i3 MK3 and WN400 3D Platform) were used for layer-by-layer manufacturing of polylactic acid (PLA) Dog Bone (DB) and Single Edge Notched Bend (SENB) specimens, aimed at investigating the influence of the manufacturing parameters on the tensile and fracture properties of PLA elements obtained by FDM technology. The effects of growing direction (horizontal and vertical), building orientation (0°, 45° and 90°), printer type, layer thickness (0.15 and 0.40 mm), specimen thickness (4 and 10 mm) and filament color (purple, white, black, gray, red, orange) are discussed in detail. Tensile tests were performed on DB specimens, while fracture mechanics tests on SENB specimens. Both the tensile and fracture properties of FDM 3D-printed PLA specimens have been found to be dependent on the investigated manufacturing parameters. From the microstructural analyses of the SENB fracture surfaces, it has been observed that the fracture mechanisms and crack propagation is a step-wise process. Finally, the material properties charts (Young's modulus and mode I fracture toughness versus tensile strength) are plotted.

1. Introduction

Additive manufacturing (AM) is a process in which components are created layer-by-layer on a special platform through computer-aided design (CAD) and manufacturing and enables the production of components with a complex geometry. The AM technology is able to print almost any material (e.g. metals and their alloys, ceramics, polymers, biological materials, etc.), offering a wide range of products in different ranges of engineering applications, such as the automotive, aerospace, civil, medical, energy, sport industries [1–4]. AM technology can be classified into different manufacturing processes including selective laser sintering (SLS), stereolithography (SLA), power fused deposition modeling (FDM), bed and inkjet head 3D printing (PIP) and liquid frozen deposition manufacturing (LFDM) [5].

The FDM technology, one of the most widely used in additive manufacturing, is based on the extrusion technique; its success is

* Corresponding authors.

E-mail addresses: cristina.valean@yahoo.com (C. Vălean), emanoil.linul@upt.ro (E. Linul).

<https://doi.org/10.1016/j.engfracmech.2022.108766>

Received 28 February 2021; Received in revised form 26 August 2022; Accepted 28 August 2022

Available online 7 September 2022

0013-7944/© 2022 The Author(s). Published by Elsevier Ltd. This is an open access article under the CC BY-NC-ND license (<http://creativecommons.org/licenses/by-nc-nd/4.0/>).

Nomenclature

a	Crack length
ABS	Acrylonitrile Butadiene Styrene
AFPB	Asymmetric Four Point Bending
AM	Additive Manufacturing
a/W	Crack length ratio
b	Width of the DB specimen in correspondence of the narrower section
b_g	Width of the DB specimen in the grip area
B	Thickness of the SENB specimen
CAD	Computer-Aided Design
CF	Carbon Fiber
CLSM	Confocal laser scanning microscopy
DB	Dog-Bone
E	Young's modulus
FDM	Fused Deposition Modeling
$f_I(a/W)$	Mode I geometry factor
$f_{II}(a/W)$	Mode II geometry factor
h	Specimen's width
K_I	Mode I stress intensity factor
K_{II}	Mode II stress intensity factor
K_{IC}	Mode I fracture toughness
K_{IIC}	Mode II fracture toughness
LFDM	Liquid Frozen Deposition Manufacturing
L_0	Gauge length of the DB specimen
L_c	Length of the narrower section of the DB specimen
L_t	Total length of the DB specimen
MTS	Maximum Tangential Stress
P	Applied load
PA	Polyamide
PC	Polycarbonate
PET	Polyethyleneterephthalate
PLA	Polylactic acid
P_{max}	Maximum load
PPS	Polyphenysulfone
Q	Shear load
R	Radius of the DB specimen
SENB	Single Edge Notched Bend
SFPB	Symmetric Four Point Bending
SLA	Stereolithography
SLS	Selective Laser Sintering
t	Layer thickness
W	Height of the SENB specimen
σ	Normal stress
σ_f	Tensile strength
τ	Shear stress

mainly due to its cost-effective way of printing and the ease of obtaining parts [6–8]. In FDM process, the 3D printing machine contains a plastic wire spool feeding a print head (nozzle) which extrudes a thin filament of melted plastic, forming, layer-by-layer according to a CAD file, the final component [9–11]. A wide range of plastic materials like polylactic acid (PLA), polycarbonate (PC), acrylonitrile butadiene styrene (ABS), polyphenysulfone (PPS), polyethyleneterephthalate (PET) and polyamide (PA) can be used for printing [12,13].

Wang et al. [14] and Feng et al. [15] investigated the mechanical properties of the parts obtained by AM technology. Previous researches have shown that the main process parameters influencing the mechanical properties are the raster orientation, and the layer thickness and nozzle temperature [16–18]. It was also observed that, in addition to the mentioned printing parameters, the color of the filament, the infill type, the building orientation and the printing direction have all a major influence on the tensile properties of PLA parts [19–21]. In addition, several studies have reported that FDM components manufactured by using PLA filaments show properties comparable to those made of bulk PLA [18,20–22]. The investigation of the tensile behavior of PC and ABS parts aimed at determining the degree of the anisotropy in 3D printed components, was carried out by Cantrell et al. [23]. They found that the raster orientation of

the PC specimens lead to an anisotropic behavior, resulting in a directional variation of up to 20% of the strengths and elastic modulus. On the other hand, the authors observed that the values of Poisson's ratio and Young's modulus for ABS are slightly influenced by the raster and build orientation. Maloch et al. [24] investigated the influence of the layer thickness and extrusion nozzle type on the tensile/flexural modulus and tensile/flexural strength of 3D-printed ABS parts. They noticed that the small thicknesses of the layers allow to obtain the best mechanical properties. They also found that an increase in nozzle temperature provide better melting between adjacent layers. The effect of the layer orientation on modulus of rupture, tensile strength and impact resistance was investigated by Es-Said et al. [25]; the best properties were obtained for an orientation of 0° (with layers build along the length of the parts), while the weakest behavior for a 45° one. In addition, the authors observed that the crack paths regularly occurred along the layer interface. Rodríguez-Panes et al. [26] investigated the tensile behavior (modulus of elasticity, tensile strength, tensile yield stress and rated tensile stress) of various PLA and ABS components produced by the FDM technique. Specimens made of PLA were found to be stiffer and with higher tensile strength than ABS. On the other hand, the results obtained with ABS showed a lower variability than those obtained with PLA. Warnung et al. [27] studied the mechanical behavior of eight types of FDM printed component; it was found that PA components exhibited the best strength properties, while the stiffest component was produced using a carbon fiber (CF) reinforced PET.

Due to its superior strength/stiffness properties, bio-based, bio-compostable, and bio-compatibility PLA thermoplastic elements are widely used in various advanced applications. Nonetheless, in addition to the high strength and stiffness of this polymeric material, its brittle behavior have been shown to limit its lifespan [28]. Due to all the above-mentioned properties, PLA material is nowadays the most used in FDM printing. A reliable and confident use of PLA elements thus requires the mechanical properties to be precisely known; among them, the fracture toughness of the components made of this material is an important parameter to study. In addition to strength properties, Ahmed and Susmel [29,30], Arbeiter et al. [31] and Seiber et al. [32] determined the fracture properties of PLA specimens. However, the literature reports only a few results for mode II and mixed mode fracture toughness of PLA parts [10,33].

The Single Edge Notched Bend (SENB) was adopted for the determination of Mode I and Mode II fracture toughness using a symmetric and an asymmetric loading configurations, respectively [34]. Particularly, the asymmetric loading was employed to determine mode II fracture toughness for different types of brittle materials [35] such as concrete [36], granite [37,38], wood [39], polyurethane foam [40–42], extruded polystyrene [43], polyamide [16], bi-material PMMA-Aluminum [44].

Starting from the published data, which are often affected by some ambiguities related to the influence of certain process parameters [11,18,45–47] on tensile and fracture toughness properties, this paper experimentally investigates the tensile and fracture properties of PLA printed specimens. In particular, this study considers the assessment of the mode II fracture toughness, a parameter not yet investigated in the literature, of FDM printed PLA elements.

2. Manufacturing process

The test specimens were fabricated via FDM using two different printers namely Prusa® i3 MK3 printer [48] and WN400 3D Platform® printer [49]. The G-codes for FDM process were generated with the help of slicer Ultimaker® Cura 4.2.1 which results to be compatible with both the adopted printers; this allows obtaining more comparable specimens for sake of experimental results comparison. The constant process parameters for fabricating the test specimens are provided in Table 1. It should be noted that Pusaent PLA filament (manufacturer PRUSA) of two different diameters (1.75 and 2.85 mm) were used for Prusa and 3D platform printers. It should be noted that the main goal of the current research is not to perform a direct comparison of the two utilized printers, as few process parameters (i.e. nozzle diameter and layer thickness are different) are not identical when producing samples using the two printers (see Table 1). As reported by Dawoud et al. [50], the raster angle of +45°/−45° for the FDM parts can result in higher mechanical and fracture resistance, hence, in the current research this raster orientation was selected for fabrication of the specimens. A nominal infill density of 100% was defined for all test specimens in order to approach as closely as possible the continuous material. To assess the effect of printing angle (in-plane angle on the build platform), different building angles equal to 0°, 45°, and 90° were considered. All the printed specimens were fabricated through the thickness for producing SENB specimens, while both through the thickness and through the width printing have been assumed for preparing SENB specimens.

For the tensile and fracture experiments, dog-bone (DB) and single edge notch bend (SENB) specimens were prepared, respectively. Fig. 1 illustrates the basic features of these two geometries. To compare the fracture resistance of the FDM parts in as-fabricated condition and in the case where the crack is introduced to the bulk material, two different sets of SENB specimens were considered. In the first type of SENB specimens, the notch was introduced in the CAD model which was used for FDM fabrication. In this case,

Table 1
Process parameters for manufacturing test specimens for tensile tests by using the two different printers.

Process parameter	Prusa® i3 MK3	3D Platform® WN400
Nozzle diameter	0.4 mm	1 mm
Infill density	100%	100%
Nozzle temperature	220 °C	220 °C
Bed temperature	60 °C	60 °C
Raster angle	+45°/−45°	+45°/−45°
Build direction	Flat, printed through the thickness	Flat, printed through the thickness
Layer thickness	0.15 mm	0.40 mm

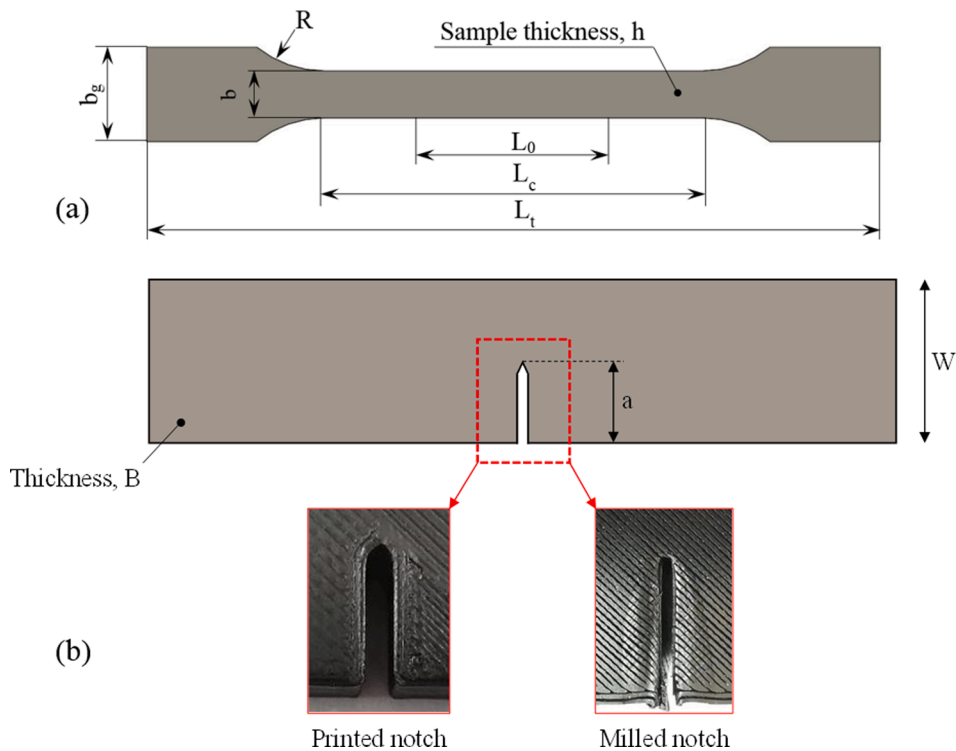


Fig. 1. Schematic illustration of PLA-FDM specimens: DB (a) and SENB (b) specimens.

the notch geometry has been introduced throughout the thickness and the two outer walls surround the notch area as well as the rest of the circumference.

In the second type of SENB specimens, prisms with the same global dimensions as the SENB specimens were fabricated and the notch geometry was introduced by milling by using a tool of 0.6 mm thickness (see Fig. 1b). During the milling process, the coolant was continuously used to prevent excessive heating of the specimen in order to reduce the change of melting and prevent recrystallization in the notched area. Microscopic investigation of the notch tip show similar shape and dimensions of the notch for both printed and milled notch, the only difference is that for printed notch the contour of the specimen is continuum, while for the milled one the deposited filaments in the notch area are cut.

3. Experimental investigations

3.1. Tensile tests

Tensile tests were performed on the 5 kN Zwick Proline Z005 testing machine, with the exception of 10 mm thick specimens which were tested on the 100 kN A009 (TC100) computerized electromechanical universal testing machine (LBG srl®). All quasi-static tests

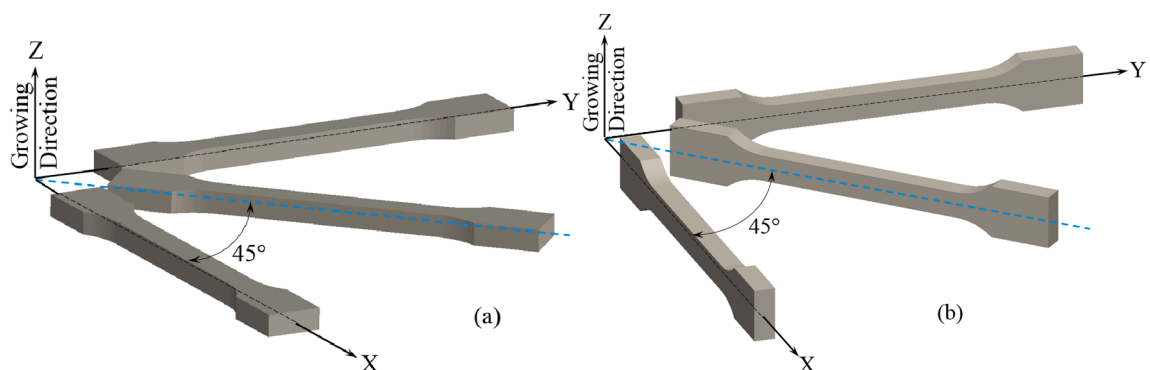


Fig. 2. Printing direction and orientation: Horizontal (through the thickness) (a) and Vertical (through the width) (b) growing.

were carried out at room temperature under displacement control, with a displacement rate of 2 mm/min. Clip-on extensometers with 30 mm measuring length were used to record the displacements used to calculate the Young modulus, in accordance with ISO 527–1 standard [51]. The tensile strength was estimated by dividing the maximum load to the cross section of the DB specimen. Five specimens were tested for each set of manufacturing parameters. The reported results are the average values.

3.1.1. Effect of growing direction and orientation

Two growing directions of horizontal (Fig. 2a) and vertical (Fig. 2b) were considered for fabrication of the test specimens. For each direction three orientations of 0°, 45° and 90° were considered.

Typical load–displacement curves recorded during tensile testing are shown in Fig. 3. A quasi-brittle fracture can be observed for the specimens grown in the vertical direction (through the width) and in the horizontal direction (through the thickness) for 45° orientation. Specimens printed in the horizontal plane and with an orientation of 0° and 90° displayed a softening behavior after the maximum load.

The results of Young modulus and tensile strength obtained for the specimens manufactured with Prusa printer for specimens with a thickness of 4 mm, and width of 10 mm are shown in Fig. 4. Higher Young modulus values were obtained for all three considered orientations for the vertical grown specimens; compared with the values related to the horizontal ones, it has been found an increase of about 3.6% for 45° orientation and approximately 6% higher for 0° orientation. Also, it could be observed that Young modulus values are not significantly influenced by the orientation, the results are in the scatter of experimental determination for both horizontal and vertical directions.

The tensile strength is higher for the horizontal grown specimens, with an increase of about 2.1% for 45° orientation and 8.8% for 90° orientation with respect to the vertical ones.

Broken DB specimens after tensile tests for both vertical and horizontal growing directions are shown in Fig. 5. It could be observed that the fracture plane for horizontal growing direction is at 45° for 0 and 90° specimen orientation, while for the 45° specimen the orientation the fracture surface is normal to the loading direction. In the case of vertical growing direction, the fracture plane is normal to the loading direction for all growing orientations (0°, 45° and 90°).

The fracture planes of the DB specimens are directly related to the orientation of the printed layers with respect to the loading direction. The 3D printed specimens were investigated after tensile tests using Confocal Laser Scanning Microscopy (CLSM). The specimens were oriented up in order to be evaluated using 3D measuring laser microscope (Lext OLS400, Olympus, Japan) for 3D characterization of the fracture surfaces. The scanning was performed at 50X magnification and the investigated areas were about 2.3 mm³. A detailed optical 3D profiles of the fracture zones are shown in Fig. 6. The images are taken from the fracture area of the DB specimens and perpendicular to the loading direction.

3.1.2. Effect of printer, layer and specimen thicknesses

Identical specimens geometries, characterized by a thickness equal to 4 and 10 mm, layer thickness of 0.15 mm (Prusa printer) and 0.40 mm (3D Platform printer), respectively, were manufactured by using the two above-mentioned printers. For this study, specimens made of black color filament grown horizontally have been prepared. A comparison of the mechanical properties in term of the Young modulus is shown in Fig. 7a, while the tensile strength is shown in Fig. 7b. It can be observed that the Young modulus increases with the specimen thickness; further, for both thicknesses higher values of approximately 7.6% were obtained for the specimens printed on 3D platform. Higher tensile strength values (+10.4% for specimens with 4 mm thickness and + 5.2% for specimens with 10 mm thickness) were obtained for Prusa printer. The tensile strength values on thicker specimens resulted to be higher of about 12% for Prusa printer, while an increase of 17.4% was observed for 3D Platform printer.

3.1.3. Effect of filament color

Different filament colors were considered for horizontal specimens grown at 0° orientation. The Young modulus and tensile strength results are shown in Fig. 8, where some results from the literature are also reported [52]. It can be observed that the maximum Young modulus was obtained for red specimens 3379.8 MPa, while the minimum one, equal to 2855.0 MPa, was obtained for the orange specimens. The highest values of tensile strength, resulted to be above 50 MPa, were observed for purple and red specimens,

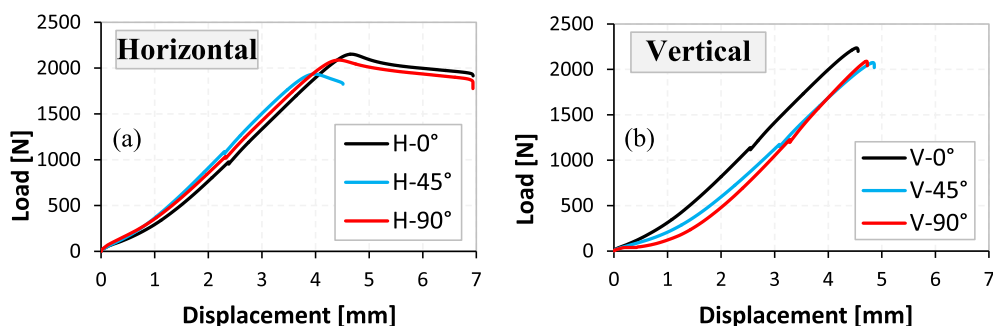


Fig. 3. Load - displacement curves obtained from the tensile tests: horizontal (a) and vertical (b) growing direction.

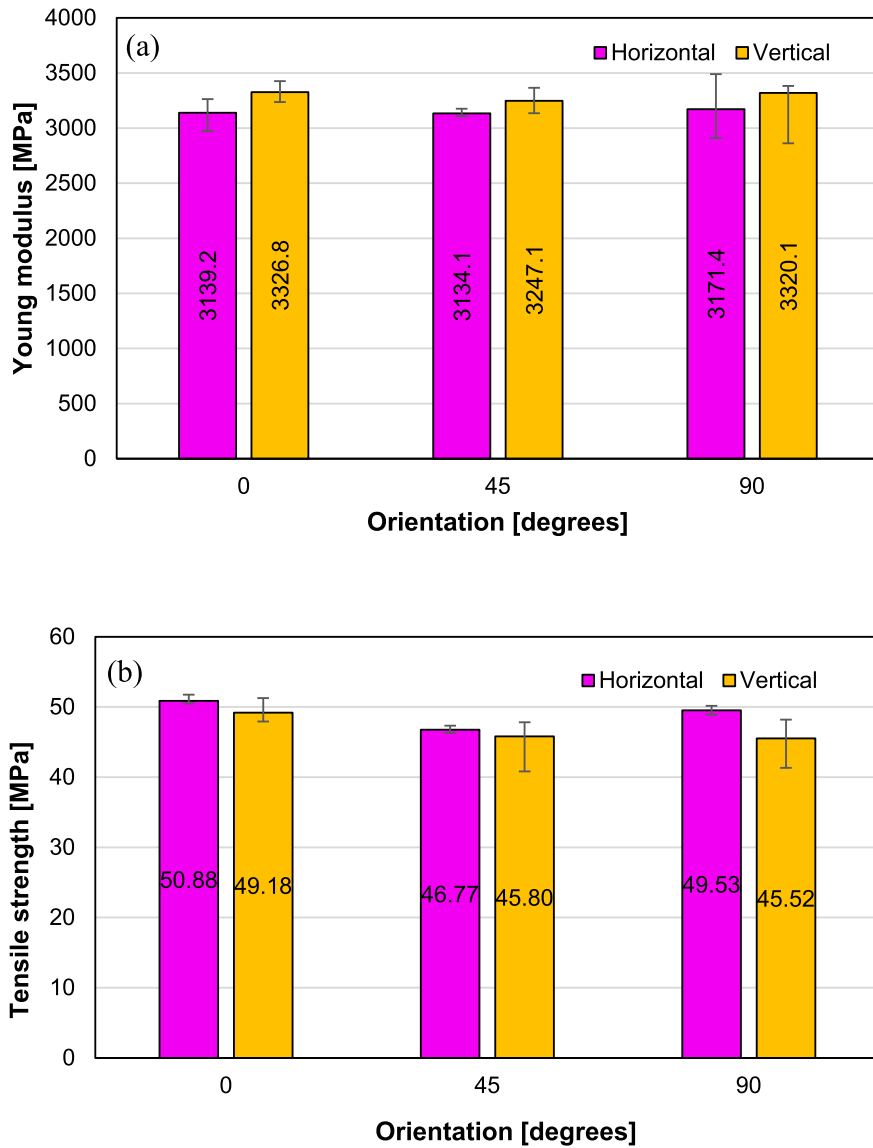


Fig. 4. The influence of growing direction and orientation on the Young modulus (a) and tensile strength (b) properties. Both average values and standard deviations are illustrated.

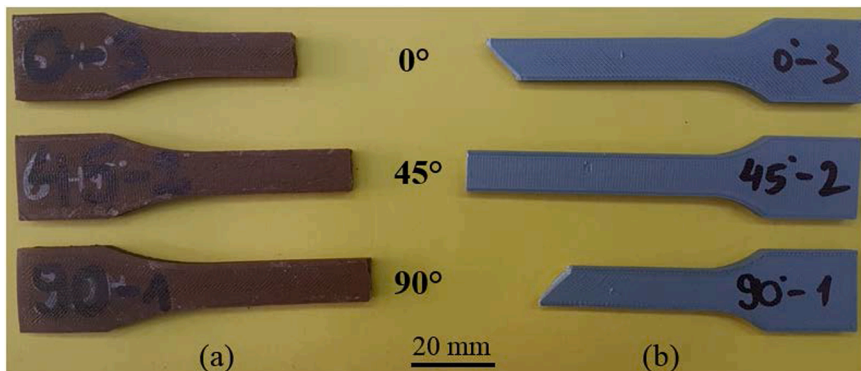


Fig. 5. Fractured DB specimens after tensile tests for vertical (a) and horizontal (b) growing directions.

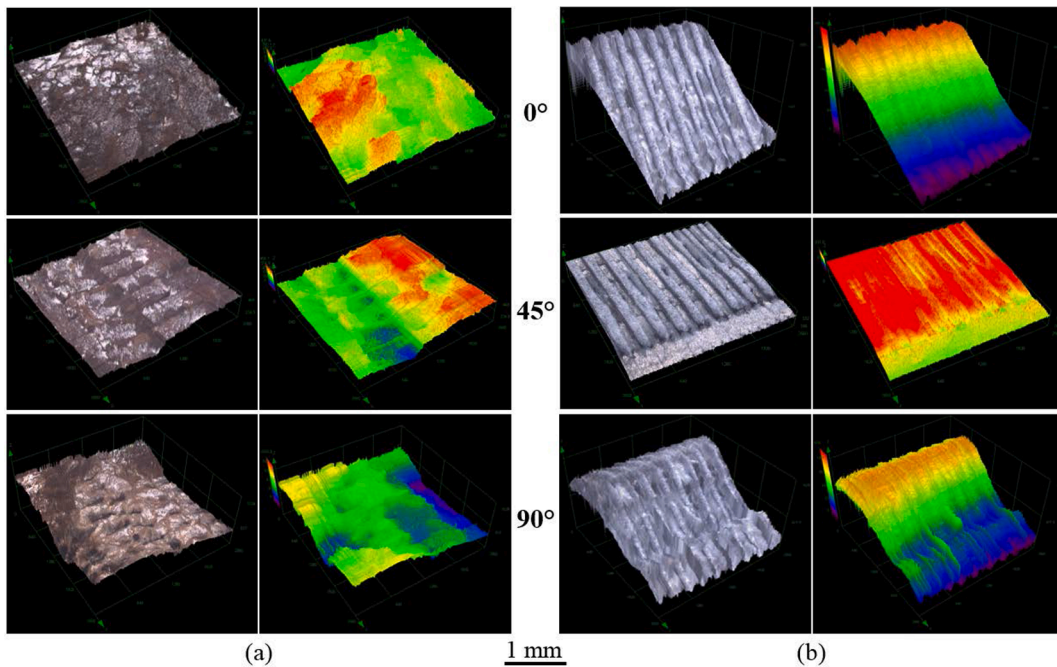


Fig. 6. Fracture planes of DB specimens for vertical (through the thickness) (a) and horizontal (through the width) (b) growing direction.

while the minimum value of 39.01 MPa was observed for the white specimens. However, further investigations into chemical composition of the coloring agent is required to accurately link the mechanical properties to the color of the PLA filament.

3.2. Fracture toughness tests

The single edge notch bend specimens (SENB) were considered for fracture toughness tests, Table 2. The specimens used for the fracture toughness tests presented two filament colors: black (10 mm thick specimens) and gray (6 mm thick specimens). In some of the specimens, the notch was created by during the 3D printing process itself, while for the un-notched specimen the notch was inserted by milling, Fig. 1b.

The fracture toughness tests were carried out at room temperature (22 °C) with a 10 kN Walter + bay hydraulic machine in displacement control with a 2 mm/min displacement rate. The mode I fracture toughness, K_{IC} , was determined using a Symmetric Four Point Bending (SFPB) configuration (Table 2a), while for the mode II fracture toughness, K_{IIC} , Asymmetric Four Point Bending (AFPB) specimens were considered (Table 2b).

The K_{IC} and K_{IIC} values were determined using the maximum load recorded during tests, P_{max} , according to Equations (1) and (4) from Table 2 [53,54].

For each set of manufacturing parameters and loading configuration, five specimens were tested. All the results presented below concerning the fracture toughness, represent the average value of the five tested specimens.

For investigating the influence of the printing direction, the specimens were printed horizontally on three directions of 0°, 45° and 90° (see Fig. 9).

Typical load–displacement curves obtained on SENB specimens for both SFPB and AFPB loadings are plotted in Fig. 10. The fracture toughness results under mode I and mode II loading conditions for different printing directions are shown in Fig. 11. It could be observed from Fig. 11 that for both modes of fracture the values of fracture toughness are higher for 0° orientation, followed by the 90° ones and the lower values correspond to 45° orientation. This trend could be observed also for the work of fracture for Mode I loading. On contrary for Mode II the highest work of fracture was observed for 45° direction. This could be explained by the influence of the raster angle on the plastic deformation around the crack tip.

The fracture paths, starting from the notch root, are presented in Fig. 12 for mode I and mode II loading. For 0° (Fig. 12a) and 90° (Fig. 12c) orientations and mode I loading, the crack initiates along the notch for the first two printing layers (outer walls), and then kink at 45° following the raster angle. For mode I loading and 45° orientation, the crack initiates and propagates along the notch bisector line. Mode II loading shows an inclined crack initiation, followed by a propagation along the raster angle. A higher fracture process zone could be observed for Mode II loading and printing orientation 45° (Fig. 12e), which could explain the higher value of the work of fracture for this case.

The fracture planes of the SENB specimens, observed for different loading modes (mode I and mode II) and growing orientations are shown in Fig. 13. It can be seen that the fracture surfaces of the specimens highlights different profiles depending on the above-mentioned parameters. A detailed optical 3D profiles of the fracture zones are shown in Fig. 6. The flattest fracture surfaces are

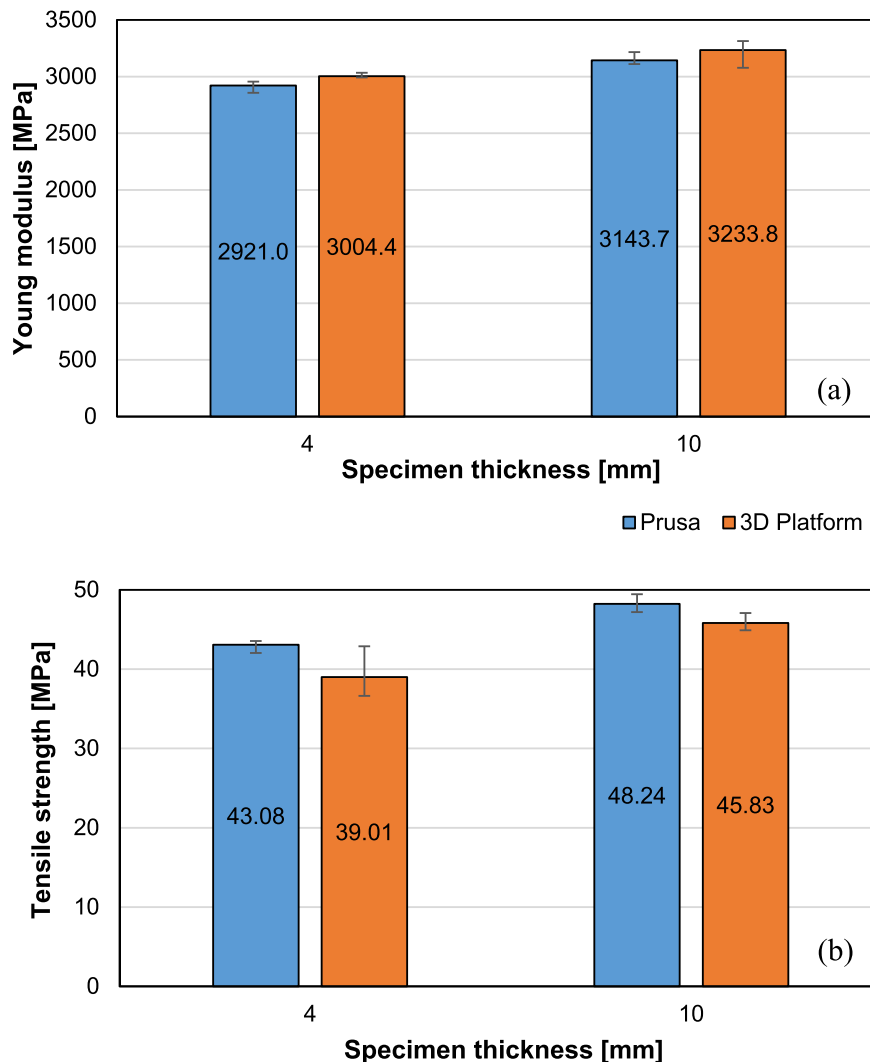


Fig. 7. Effect of DB specimen thickness and 3D printer on the Young modulus (a) and tensile strength (b) properties.

obtained for a printing orientation at 45° , while the other two printing directions (0° and 90°) have quite irregular profiles. In fact, these optical profiles reinforce the shape of the fracture paths obtained at the macroscopic level (see Fig. 12).

The experimental result for the considered manufacturing parameters, the two printers (Prusa and 3D platform) printing layers of 0.15 mm and 0.40 mm, respectively, specimens with two different thicknesses 10 and 6 mm and two methods to insert the notch (by 3D printing or through mechanical cutting using milling), are presented in Table 3 for mode I fracture toughness and in Table 4 for mode II fracture toughness, respectively. The lowest value of the K_{IC} was obtained for specimens with 3D printed notch on 10 mm thickness specimens, followed by the specimens with milled notch. The mode I fracture toughness for specimens obtained on 3D platform printer (0.4 mm layer thickness) are higher than those obtained on Prusa printer. The same tendency was observed for mode II fracture toughness (Table 4). Almost similar values of $K_{IIC} = 3 \text{ MPa}\cdot\text{m}^{0.5}$ were obtained on specimens manufactured on Prusa printer with 3D printed notch for different thicknesses (6 and 10 mm). The lowest K_{IIC} was obtained for Prusa printed specimens with milled notch.

From the results reported in Tables 3 and 4 it appears that a smaller specimen's thickness results in higher fracture toughness, while using thinner layer entails a reduction of the fracture toughness because of the more numerous stress raiser sites induced by the alternating printed layers. On contrary with the tensile tests results where higher tensile strain was obtained for thicker specimens, we should notice that the thicker specimens are close to plain strain conditions, while the thinner ones are in plan stress conditions.

Fig. 14 presents the influence of the fracture parameters on the ratio between mode II and mode I fracture toughness. It could be observed that K_{IIC}/K_{IC} ranges between 0.55 and 0.59 for 3D platform printer and between 0.57 and 0.74 for Prusa printer, respectively.

4. Discussions and conclusions

We have investigated the influence of some manufacturing parameters on the tensile and fracture properties of PLA specimens

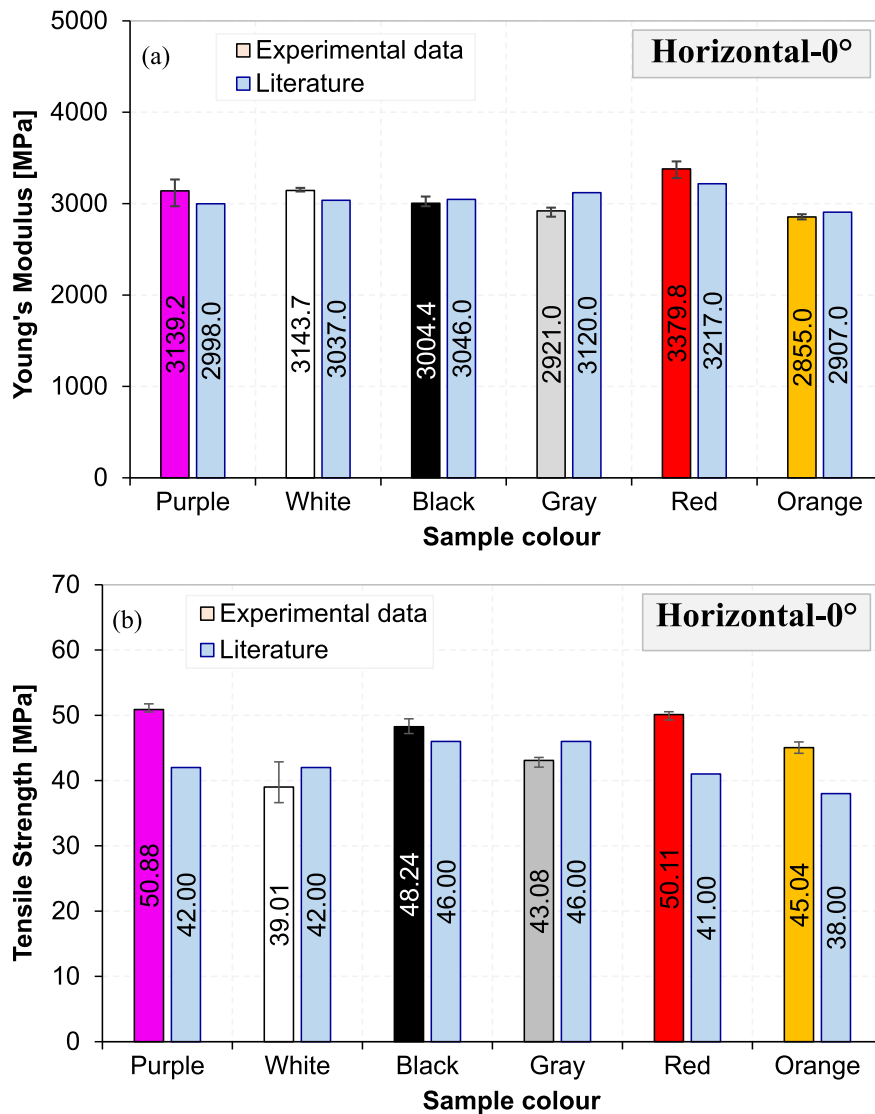


Fig. 8. Effect of filament color on the Young modulus (a) and tensile strength (b) properties of PLA printed elements.

obtained via FDM technique.

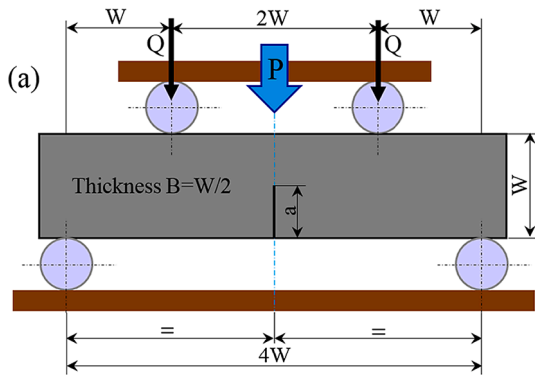
Higher stiffness was obtained for vertical growing direction, higher ultimate tensile strength was obtained for horizontal direction, respectively. Tensile tests results highlighted the influence of specimen orientation, layer thickness and filament color on Young modulus and tensile strength.

According to the experimental results, the fracture resistance of specimens printed with different orientations is strongly dependent on the manufacturing parameters. In this scenario, the specimens printed with 45° orientation are characterized by a lower K_{IC} values, while higher values were obtained for the specimens printed with 0° and 90° orientations. This behavior can be explained by having a clear understanding of the effect of the angle between the pre-crack in the specimens and the raster lines. This angle is equal to $\pm 45^\circ$, $0^\circ/90^\circ$ and $\pm 45^\circ$ for the printed SENB specimens with 0° , 45° , and 90° build orientations. Considering mode I loading for 0° and 90° orientations, if the crack tries to propagate along the bisector line it should break two sets of inclined fibers with $\pm 45^\circ$ angles. On the other hand, if the crack propagates along 45° direction, there is only one set of fiber (half of the number of resistant fibers) preventing the crack growth. This can be the reason for crack propagation along the 45° direction in 0° and 90° specimens, and the 0° propagation direction for 45° specimens (see Fig. 10).

Although the specimens are loaded under mode I, the presence of the inclined rasters in 0° and 90° specimens causes the crack path not to follow the same path as in an isotropic material. In this case, since the crack would like to propagate along the notch bisector line but is forced to follow the 45° raster, and due to the local mixed mode loading condition ahead of the crack tip, higher amount of plastic deformation is expected. This shielding effect results in higher load bearing capacity and also higher elongation at failure (see Fig. 8a).

Regarding the 45° specimens with $0^\circ/90^\circ$ angle between the rasters and the pre-crack, the crack propagation occurs along the

Table 2
Schematic of SFPB and AFPB test and the K_{IC} and K_{IIC} relations [53].

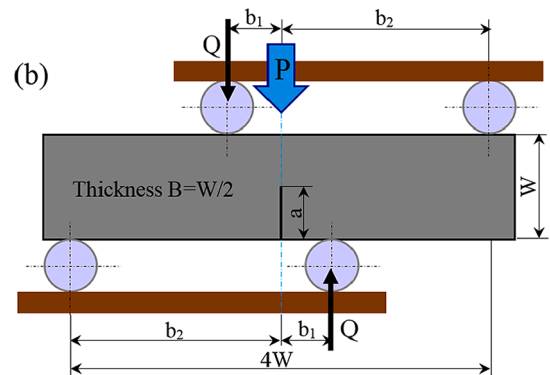


SFPB configuration

$$K_{IC} = \sigma\sqrt{\pi a} \cdot f_I\left(\frac{a}{W}\right)$$

with $\sigma = \frac{3P_{max}}{BW}$

$$f_I\left(\frac{a}{W}\right) = 1.122 - 1.121\left(\frac{a}{W}\right) + 3.74\left(\frac{a}{W}\right)^2 + 3.873\left(\frac{a}{W}\right)^3 - 19.05\left(\frac{a}{W}\right)^4 + 22.55\left(\frac{a}{W}\right)^5$$



AFPB configuration

$$(1) \quad K_{IIC} = \tau\sqrt{\pi a} \cdot f_{II}\left(\frac{a}{W}\right) \tag{4}$$

$$(2) \quad \text{with } \tau = \frac{Q}{BW}, \quad Q = P_{max} \frac{b_2 - b_1}{b_2 + b_1} \tag{5}$$

$$(3) \quad f_{II}\left(\frac{a}{W}\right) = -0.2915 + 6.3229\left(\frac{a}{W}\right) - 9.12\left(\frac{a}{W}\right)^2 + 6.057\left(\frac{a}{W}\right)^3 \tag{6}$$

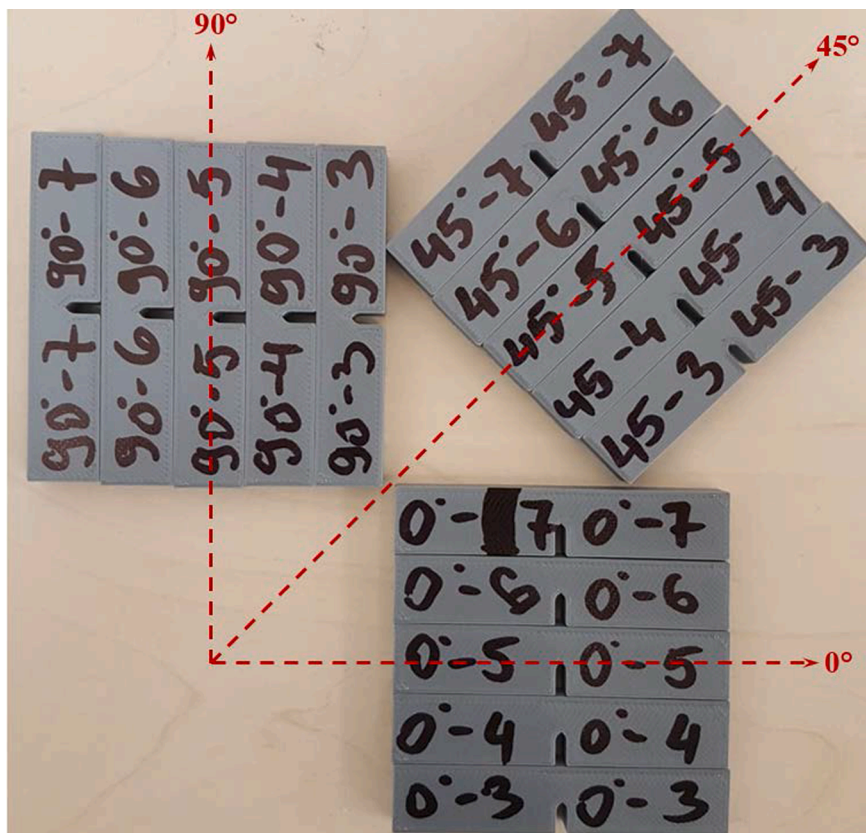


Fig. 9. Printed SENB specimens on the three considered orientations (0°, 45° and 90°).

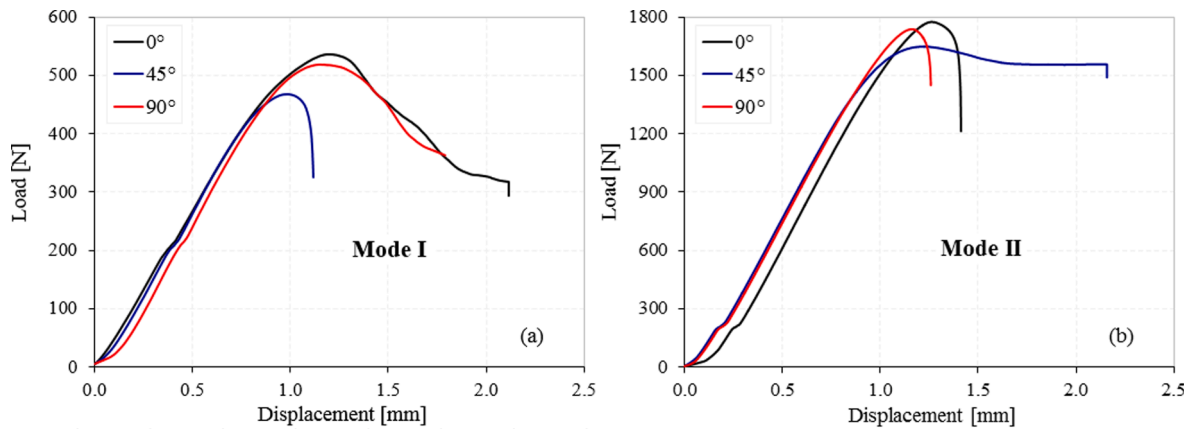


Fig. 10. Load-displacement curves for SFPB (a) and AFPB (b) fracture tests.

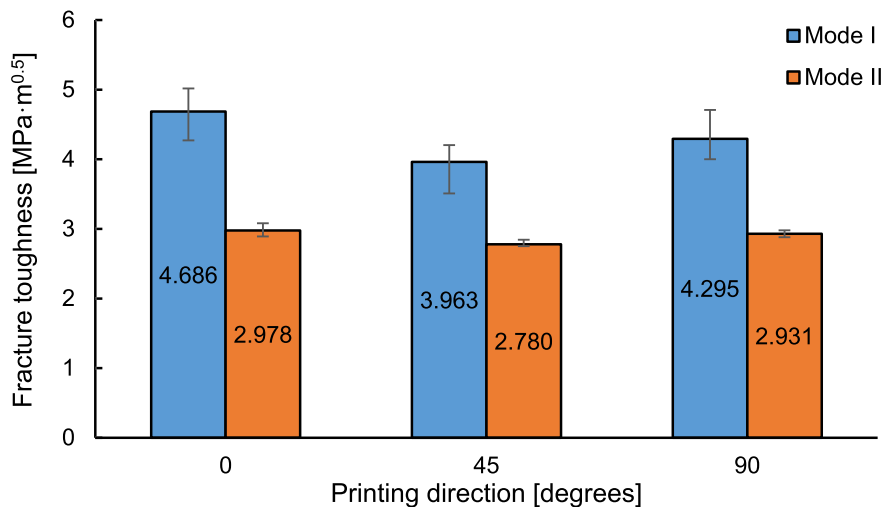


Fig. 11. The influence of the specimen orientation on the K_{IC} and K_{IIC} .

symmetric induced stress field in the specimens. In this case, the crack growth resistance is lower and it can be observed that the fracture happens at lower load and a lower elongation at failure is observed (see Fig. 8a).

Dealing with mode II loading condition, the major difference in the tested cases is the elongation at failure, while the K_{IIC} shown smaller variations among various cases. According to the Maximum Tangential Stress (MTS) criterion, the crack kinking angle for an isotropic material is about 70.5° [55]. Using the same argument as the mode I results, in the specimens where the angle between the maximum tangential stress and the raster angles is smaller, the crack resistance is expected to be lower. Considering an angle of 70.5° for the maximum tangential stress, this angle would be equal to 19.5° for 45° specimens and 25.5° for 0 and 90° specimens, resulting in slightly lower K_{IIC} value for 45° specimens.

The presence of the outer walls of the specimen is very important when it comes improving the mechanical properties. Regardless of the loading mode, in order the crack to growth inside the bulk material, it must break and propagate through these walls. When the notch is created by milling, the outer walls do not exist in the notch region, meaning that this barrier is removed, making for the crack easier to start propagating under a lower load level. This has resulted in lower fracture toughness values for the milled specimens (see Tables 3 and 4). One important point for the milled notches is the higher standard deviation for the fracture toughness observed in these specimens. The presence of the uniform outer wall is an element making the specimens be in almost same outer condition.

By removing that wall, any factor can be amplified, and possibly large defects within the bulk material and changes of temperature during the milling can be responsible for a huge scattering of the measured quantities.

By looking at the fracture surface (Figs. 6 and 13), a clear trend of the fiber failure can be observed; it can be appreciated that the fibers were the load bearing members in the specimens. In this scenario, having larger fibers for the same volume of the specimens, can improve the load bearing of the element. The fracture and crack propagation take place as a step-wise process. If in each step a thicker fiber has to be broken for the crack to propagate, it would require a higher applied load, which consequently results in a higher fracture toughness. The other possible explanation can be the crystallization taking place during and after the printing. Depending on the

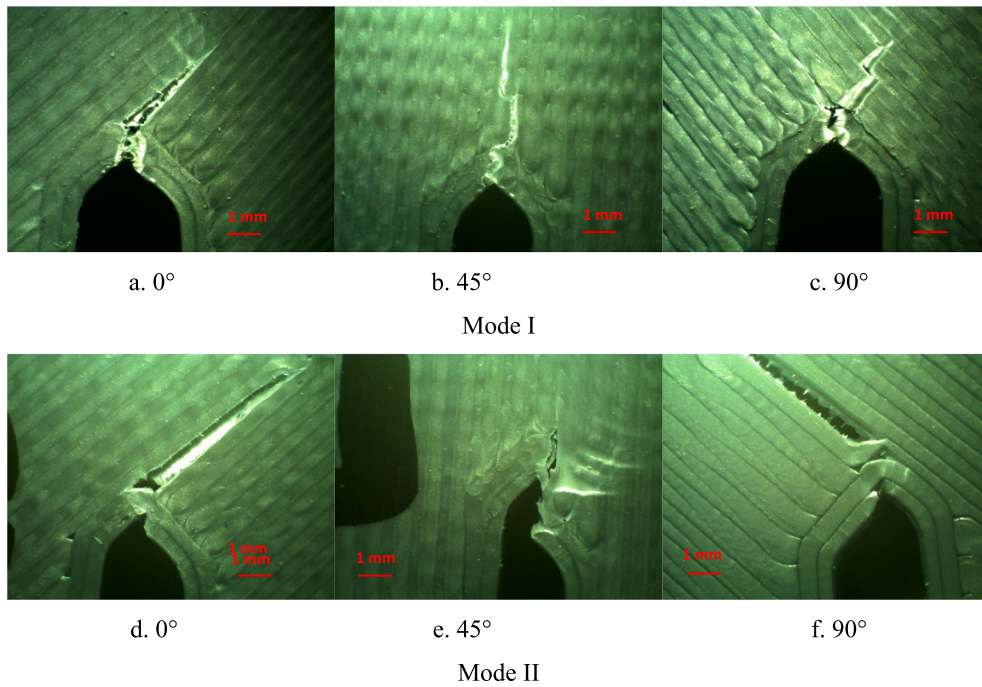


Fig. 12. Fracture paths after mode I and mode II loading tests.

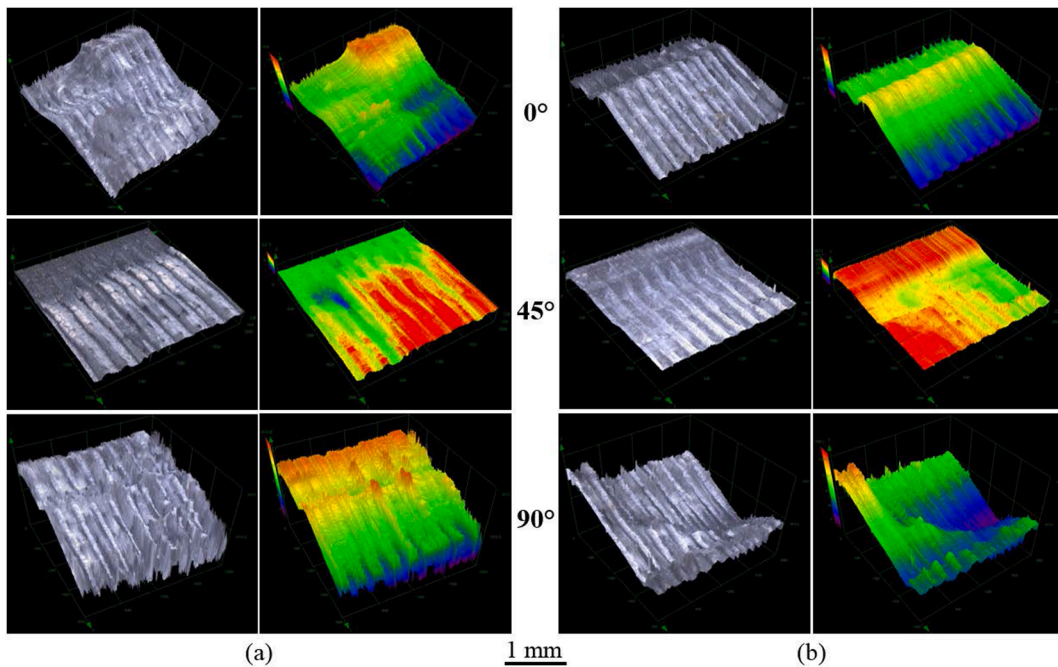


Fig. 13. Fracture planes of SENB specimens for mode I (a) and mode II (b) test.

printing speed, layer height and some other parameters, the heat history can be different in FDM parts. If the average induced heat (residual heat) in the larger parts has been higher, that could result in higher mechanical properties and better bonding of the layers.

For a general overview of the interaction between the main mechanical and fracture properties of PLA components, a chart of the material properties – drawn according to [56] – are plotted in Fig. 15. In Fig. 15a the relationship between the Young modulus E and tensile strength σ_f (for the two different printers, specimen thicknesses and specimen orientations) together with the design lines: $M_1 = \sigma_f^2/E$, with $M_1 = 0.5MPa$ (solid line) and $1MPa$ (dotted line) is shown.

Table 3
Mode I fracture toughness results.

Number	Manufacturing parameters					K_{IC} , [MPa·m ^{0.5}]	
	Printer	Notch manufacturing	Layer thickness, t [mm]	Specimen Thickness, h [mm]	Printing orientation [°]	Average	Standard deviation
1	3D Platform	3D printed	0.40	10	0	6.54	0.030
2	3D Platform	Milled	0.40	10	0	5.77	0.399
3	Prusa	3D printed	0.15	10	0	4.07	0.202
4	Prusa	Milled	0.15	10	0	4.25	0.290
5	Prusa	3D printed	0.15	6	0	4.69	0.350

Table 4
Mode II fracture toughness results.

Number	Manufacturing parameters					K_{IIc} , [MPa·m ^{0.5}]	
	Printer	Notch manufacturing	Layer thickness, t [mm]	Specimen Thickness, h [mm]	Printing orientation [°]	Average	Standard deviation
1	3D Platform	3D printed	0.40	10	0	3.58	0.030
2	3D Platform	Milled	0.40	10	0	3.38	0.399
3	Prusa	3D printed	0.15	10	0	3.00	0.201
4	Prusa	Milled	0.15	10	0	2.43	0.290
5	Prusa	3D printed	0.15	6	0	2.98	0.083

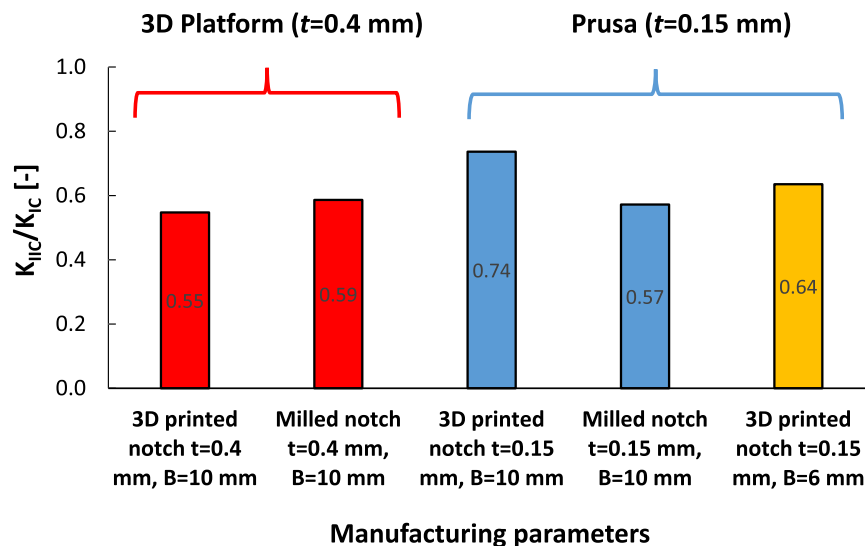


Fig. 14. Ratio between mode II and mode I fracture toughness for specimens obtained by using the two different printers and by considering printed and milled notches.

Fig. 15b shows the fracture toughness-tensile strength relationship, together with the two design curves defined as $M_2 = K_{IC}/\sigma_f$ and $M_3 = K_{IC}^2/\sigma_f$. The results related to the 3D platform fit well with the M_3 equation (dotted line) for $M_3 = 1MPa\text{Å} \cdot m$, while the ones from Prusa printer are in good agreement with the M_2 equation (solid line) for $M_2 = 0.1m^{0.5}$. This correlations are also influenced by the printing parameters, like different nozzle and layer sizes.

CRediT authorship contribution statement

Liviu Marşavina: Writing – review & editing, Writing – original draft, Supervision, Resources, Investigation, Funding acquisition, Conceptualization. **Cristina Vălean:** Writing – original draft, Investigation, Formal analysis, Data curation. **Mihai Mărghitaş:** Writing – original draft, Resources, Methodology, Formal analysis. **Emanoil Linul:** Writing – review & editing, Writing – original draft, Methodology, Investigation, Formal analysis, Data curation, Conceptualization. **Seyed Mohammad Javad Razavi:** Writing – review &

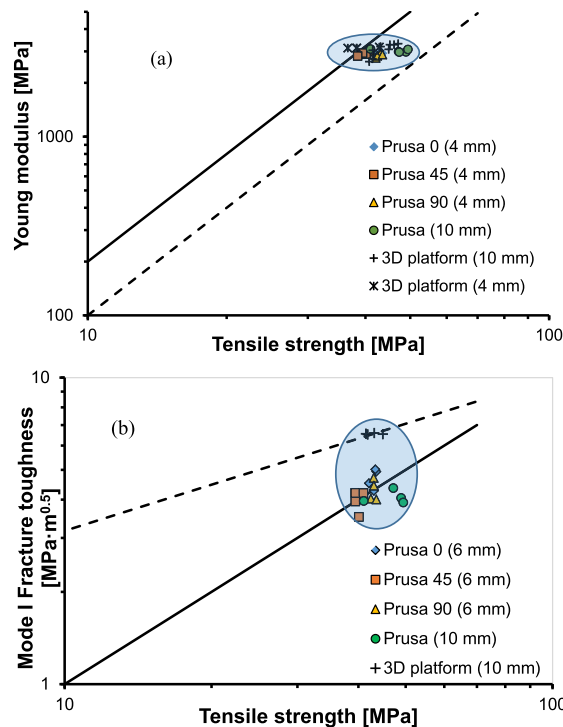


Fig. 15. Design diagrams for PLA material. Young modulus versus tensile strength; design lines for $M_1 = 1$ (dotted line) and $M_1 = 0.5$ (solid line) are shown (a). Mode I fracture toughness versus tensile strength (b). Design lines for M_2 (solid line) and M_3 (dotted line) are illustrated.

editing, Writing – original draft, Investigation, Resources. **Filippo Berto:** Writing – review & editing, Writing – original draft, Visualization, Supervision, Formal analysis. **Roberto Brighenti:** Writing – review & editing, Writing – original draft, Resources, Methodology, Formal analysis.

Declaration of Competing Interest

The authors declare that they have no known competing financial interests or personal relationships that could have appeared to influence the work reported in this paper.

Acknowledgement

The project leading to these results has received funding from the European Union's Horizon 2020 research and innovation program (H2020-WIDESPREAD-2018, SIRAMM) under grant agreement No. 857124 and was supported by a grant of the Ministry of Education and Research, CNCS/CCCDI - UEFISCDI, project number PN-III-P3-3.6-H2020-2020-0079. The authors would like to thank Christer Westum Elverum for his help during the fabrication of the test specimens using 3D Platform printer.

References

- [1] García Plaza E, López PJN, Torija MÁC, Muñoz JMC. Analysis of PLA geometric properties processed by FFF additive manufacturing: Effects of process parameters and plate-extruder precision motion. *Polymers* 2015;11:1581.
- [2] Stoia DI, Linul E, Marşavina L. Influence of manufacturing parameters on mechanical properties of porous materials by Selective Laser Sintering. *Materials* 2019; 12(6):871.
- [3] Stoia DI, Marşavina L, Linul E. Correlations between process parameters and outcome properties of Laser-Sintered Polyamide. *Polymers* 2019;11(11):1850.
- [4] Brighenti R, Cosma MP, Marsavina L, et al. Laser-based additively manufactured polymers: a review on processes and mechanical models. *J Mater Sci* 2021;56: 961–98.
- [5] Hung KC, Tseng CS, Hsu SH. 3D printing of polyurethane biomaterials. *Adv Polyurethane Biomater* 2016:149–70.
- [6] Singh S, Ramakrishna S, Berto F. 3D Printing of polymer composites: A short review. *Design Process Comm* 2020;2(2):e97.
- [7] Zhao Y, Chen Y, Zhou Y. Novel mechanical models of tensile strength and elastic property of FDM AM PLA materials: experimental and theoretical analyses. *Mater Des* 2019;181:108089.
- [8] Ben Ali N, Khelif M, Hammami D, Bradai C. Mechanical and morphological characterization of spherical cell porous structures manufactured using FDM process. *Eng Fract Mech* 2019;216:106527.
- [9] Masood SH. Intelligent rapid prototyping with fused deposition modelling. *Rapid Prototyping J* 1996;2(1):24–33.
- [10] Vălean C, Marşavina L, Mărghiţaş M, et al. The effect of crack insertion for FDM printed PLA materials on Mode I and Mode II fracture toughness. *Procedia Struct Integrity* 2020;28:1134–9.

- [11] Mohamed OA, Masood SH, Bhowmik JL. Optimization of fused deposition modeling process parameters: a review of current research and future prospects. *Adv Manuf* 2015;3(1):42–53.
- [12] Ayatollahi MR, Nabavi-Kivi A, Bahrami B, et al. The influence of in-plane raster angle on tensile and fracture strengths of 3D-printed PLA specimens. *Eng Fract Mech* 2020;237:107225.
- [13] Bahrami B, Ayatollahi MR, Sedighi I. The effect of in-plane layer orientation on mixed-mode I-II fracture behavior of 3D-printed poly-carbonate specimens. *Eng Fract Mech* 2020;231:107018.
- [14] Wang X, Zhao L, Fuh JYH, Lee HP. Effect of porosity on mechanical properties of 3D printed polymers: experiments and micromechanical modeling based on X-ray computed tomography analysis. *Polymers* 2019;11:1154.
- [15] Feng L, Wang Y, Wei Q. PA12 powder recycled from SLS for FDM. *Polymers* 2019;11:727.
- [16] Linul E, Marsavina L, Stoia DI. Mode I and II fracture toughness investigation of Laser-Sintered Polyamide. *Theor Appl Fract Mech* 2020;106:102497.
- [17] Stoia DI, Marsavina L, Linul E. Mode I fracture toughness of polyamide and alumide samples obtained by Selective Laser Sintering additive process. *Polymers* 2020;12:640.
- [18] Gordon AP, Torres J, Cole M, et al. An approach for mechanical property optimization of fused deposition modeling with polylactic acid via design of experiments. *Rapid Prototyping J* 2016;22(2):1–18.
- [19] Kiendl J, Gao C. Controlling toughness and strength of FDM 3D-printed PLA components through the raster layout. *Compos Part B* 2020;180:107562.
- [20] Yao T, Ye J, Deng Z, et al. Tensile failure strength and separation angle of FDM 3D printing PLA material: experimental and theoretical analyses. *Compos Part B* 2020;188:107894.
- [21] Vălean C, Marşavina L, Mărghitaş M, et al. Effect of manufacturing parameters on tensile properties of FDM printed specimens. *Procedia Struct Integrity* 2020; 26:313–20.
- [22] Farah S, Anderson DG, Langer R. Physical and mechanical properties of PLA, and their functions in widespread applications – a comparative review. *Adv Drug Deliv Rev* 2016;107:367–92.
- [23] Cantrell J, Rohde S, Damiani D. Experimental characterization of the mechanical properties of 3D-printed ABS and Polycarbonate parts. *Rapid Prototyping J* 2017;23(4):811–24.
- [24] Maloch J, Hnátková E, Žaludek M, Krátký P. Effect of processing parameters on mechanical properties of 3D printed samples. *Mater Sci Forum* 2018;919:230–5.
- [25] Es-Said OS, Foyos Y, Noorani R, et al. Effect of layer orientation on mechanical properties of rapid prototyped samples. *Mater Manuf Process* 2000;15(1):107–22.
- [26] Rodríguez-Panes A, Claver J, Camacho AM. The influence of manufacturing parameters on the mechanical behaviour of PLA and ABS pieces manufactured by FDM: a comparative analysis. *Materials* 2018;11:1333.
- [27] Warnung L, Estermann S, Reisinger A. Mechanical properties of fused deposition modeling (FDM) 3D printing materials. *RTEjournal - Fachforum für Rapid Technologien* 2018;(1).
- [28] Sennan P, Pumchusak J. Improvement of mechanical properties of poly(lactic acid) by elastomer. *The Malaysian J Anal Sci* 2014;18(3):669–75.
- [29] Ahmed AA, Susmel L. A material length scale-based methodology to assess static strength of notched additively manufactured polylactide (PLA). *Fatig Fract Eng Mater Struct* 2018;41(10):2071–98.
- [30] Ahmed AA, Susmel L. Static assessment of plain/notched polylactide (PLA) 3D-printed with different infill levels: Equivalent homogenised material concept and Theory of Critical Distances. *Fatig Fract Eng Mater Struct* 2019;42(4):883–904.
- [31] Arbeiter F, Spoerk M, Wiener J, et al. Fracture mechanical characterization and lifetime estimation of near homogeneous components produced by fused filament fabrication. *Polym Test* 2018;66:105–13.
- [32] Seiber P, Razavi SMJ, Susmel L, et al. Validation of the averaged strain energy density criterion for additively manufactured notched polylactide acid specimens. *Procedia Struct Integrity* 2020;28:2099–103.
- [33] Khan AS, Ali A, Hussain G, Ilyas M. An experimental study on interfacial fracture toughness of 3-D printed ABS/CF-PLA composite under mode I, II, and mixed-mode loading. *J Thermoplast Compos Mater* 2019:1–24.
- [34] Ayatollahi MR, Aliha MRM. On the use of an anti-symmetric four-point bend specimen for mode II fracture experiments. *Fatig Fract Eng Mater Struct* 2011;34: 898–907.
- [35] Aliha MRM, Mousavi SS, Ghoreishi SMN. Fracture load prediction under mixed mode I + II using a stress based method for brittle materials tested with the asymmetric four-point bend specimen. *Theor Appl Fract Mech* 2019;103:102249.
- [36] Yin Y, Qiao Y, Hu S. Four-point bending tests for the fracture properties of concrete. *Eng Fract Mech* 2019;211:371–81.
- [37] Razavi SMJ, Aliha MRM, Berto F. Application of an average strain energy density criterion to obtain the mixed mode fracture load of granite rock tested with the cracked asymmetric four-point bend specimens. *Theor Appl Fract Mech* 2017;97:419–25.
- [38] Wang C, Zhu ZM, Liu HJ. On the I-II mixed mode fracture of granite using four-point bend specimen. *Fatig Fract Eng Mater Struct* 2016;39(10):1193–203.
- [39] de Moura MFSP, Silva MAL, Morais JLL, Dourado N. Mode II fracture characterization of wood using the Four-Point End-Notched Flexure (4ENF) test. *Theor Appl Fract Mech* 2018;98:23–9.
- [40] Marsavina L, Constantinescu DM, Linul E, et al. Experimental and numerical crack paths in PUR foams. *Eng Fract Mech* 2016;167:68–83.
- [41] Apostol DA, Stuparu F, Constantinescu DM, et al. Experimental and XFEM Analysis of Mode II Propagating Crack in a Polyurethane Foam. *Materiale Plastice* 2016;53(4):685–8.
- [42] Apostol DA, Stuparu F, Constantinescu DM, et al. Crack length influence on stress intensity factors for the asymmetric four-point bending testing of a polyurethane foam. *Materiale Plastice* 2016;53(2):280–2.
- [43] Yoshihara H, Maruta M. Mode I J-integral of extruded polystyrene measured by the four-point single-edge notched bending test. *Eng Fract Mech* 2019;222: 106716.
- [44] Marsavina L, Piski T. Bimaterial Four Point Bend Specimen with Sub-Interface Crack. *Int J Fract* 2010;164:325–32.
- [45] Heidari-Rarani M, Ezati N, Sadeghi P, Badrossamay MR. Optimization of FDM process parameters for tensile properties of polylactic acid specimens using Taguchi design of experiment method. *J Thermoplast Compos Mater* 2020:1–18.
- [46] Mohamed OA, Masood SH, Bhowmik JL. Mathematical modeling and FDM process parameters optimization using response surface methodology based on Q-optimal design. *Appl Math Model* 2016;40:10052–73.
- [47] Dey A, Yodo N. A systematic survey of FDM process parameter optimization and their influence on part characteristics. *J Manuf Mater Process* 2019;3:64.
- [48] <https://www.prusa3d.com/product/original-prusa-i3-mk3s-kit-3/>.
- [49] <https://www.3dplatform.com/3D-Printers>.
- [50] Dawoud M, Taha I, Ebeid SJ. Mechanical behaviour of ABS: an experimental study using FDM and injection moulding techniques. *J Manuf Process* 2016;21: 39–45.
- [51] ISO 527-1. *Plastics-Determination of Tensile Properties-part 1: General Principles*. International Organization for Standardization; ISO: Geneva, Switzerland, 2012; 23.
- [52] Pandzic, A, Hodzic, D, Milovanovic, A. Influence of material color on mechanical properties of PLA material in FDM technology, *Proceedings of the 30th DAAAM International Symposium, Vienna, 2019*.
- [53] Murakami Y. *Stress Intensity Factors Handbook*. New York: Pergamon Press; 1987.
- [54] Linul E, Marsavina L. Prediction of fracture toughness for open cell polyurethane foams by finite element micromechanical analysis. *Iran Polym J* 2011;20(9): 736–46.
- [55] Erdogan F, Sih GC. On the crack extension in plates under plane loading and transverse shear. *J Basic Engr* 1963;85:519–25.
- [56] Ashby, M. F., *Materials Selection in Mechanical Design, Fourth Edition*, Butterworth – Heinemann, Oxford, 2011.